Deep Ultraviolet Plasmonics Using Momentum-Resolved Electron Energy Loss Spectroscopy

by

Zohreh Poursoti

A thesis submitted in partial fulfillment of the requirements for the degree of

Doctor of Philosophy

in

Photonics and Plasmas

Department of Electrical and Computer Engineering
University of Alberta

Abstract

Plasmonics deals with the collective excitations of light coupled with free electrons in matter. It has widespread use in the fields of biosensing and nanoscale waveguiding due to the enhancement of the electric fields. My thesis deals with an important frontier in the field of plasmonics by analyzing excitations in the deep ultra-violet (DUV) and extreme ultra-violet (EUV) spectral region. Specifically, I have employed a unique experimental method to probe light-matter interaction in the DUV and EUV regimes beyond the spectral range of conventional probes such as ellipsometers. One long-term outcome of my work is to propose new sources of light in this regime where we envision future applications such as DUV and EUV lithography. For this purpose, I have employed a unique momentum-resolved electron energy loss spectroscopy (q-EELS) technique to probe photonic modes in thin films at DUV and EUV energy scales. This thesis presents the theory and experimental results related to q-EELS of semiconductor thin films. EELS deals with the measurement of energy loss of relativistic electrons in a transmission electron microscope (TEM). Our technique, q-EELS is an important advancement that measures not only the energy loss but also the momentum loss of electrons thus giving insight on phenomena such as Cherenkov radiation. For the first time, we show the existence of DUV plasmons in Germanium, opening the possibility of using semiconductor materials as new plasmonic light sources. In addition, we analyze excitations in the extreme-ultra-violet regime in silicon and the temperature dependent characteristics of these high energy plasmonic excitations.

Preface

Some of the research conducted for this thesis consists of work that has been previously published in peer reviewed journals and are included in chapter 3 of this thesis:

- Zohreh Poursoti, Wenbo Sun, Sathwik Bharadwaj, Marek Malac, Suraj Iyer, Farhad Khosravi, Kai Cui, Limei Qi, Neda Nazemifard, Ravichandra Jagannath, Rajib Rahman, Zubin Jacob, "Deep ultra-violet plasmonics: exploiting momentum-resolved electron energy loss spectroscopy to probe germanium', Optics Express 30.8 (2022): 12630-12638.

Some of the research conducted for this thesis forms part of an international research collaboration, lead by Professor Zubin Jacob at Purdue University. The electron energy loss experiment was done at NRC-NANO at the University of Alberta in collaboration with Dr. Marek Malac. I was responsible for conducting electron energy loss spectroscopy experiment, the data collection, data analysis and related simulations. Sample fabrication was performed by Dr. Kai Cui at NRC-NANO via focused ion beam milling. The DFT simulation were performed by Wenbo Sun at Purdue University.
All of the work presented in this thesis is result of a collaboration from the following institutions:

- University of Alberta, Department of Electrical and Computer Engineering, 9107 - 116 Street, T6G 2V4, Edmonton, Canada,

- Nanotechnology Research Centre, National Research Council, 11421 Saskatchewan Dr NW, T6G 2M9, Edmonton, Alberta, Canada, and
- Birck Nanotechnology Center, School of Electrical and Computer Engineering, Purdue University, West Lafayette, IN 47906, USA

To my love, Arash,

for his kind heart and unwavering support.

To my parents,

for their encouragement and having faith in me.

Acknowledgements

First and foremost I would like to express my sincerest gratitude to my supervisor Prof. Zubin Jacob. His passion for science, immeasurable knowledge and insightful thinking is what made the entirety of this thesis possible. Zubin's consistent guidance and encouraging words has undoubtedly been the core influence in my academic achievements and has immensely helped me to gain confidence as a researcher and for that, I'm indebted to him.

I would like to equally extend my deepest appreciation to Prof. Marek Malac, for opening his lab to me and mentoring me to navigate through the theoretical and experimental aspects of the complex set up in the electron microscopy/spectroscopy lab. His unparalleled depth of knowledge in the field and extensive experimental skills has lead to the completion of this research work.

I would like to thank my co-advisor Prof. Sandipan Pramanik, for overseeing my work and providing support and invaluable feedback. My gratitude also goes to my committee members, Professors Manisha Gupta and Xihua Wang, for their time serving on my committee and for their feedback and suggestions.

I have had the pleasure of collaborating with Dr. Sathwik Bharadwaj and Wenbo Sun, whom I'm very grateful for. I would like to acknowledge in particular, my colleague Dr. Prashant Shekhar, who mentored me during his last year of PhD and generously provided his knowledge and expertise. Special thanks to my friends and colleagues Dr. Farid Kalhor, Dr. Saman Jahani and Dr. Farhad Khosravi, for their friendship and our discussions on science and more.

I am very appreciative of the staff of NRC NANO, in particular Dr. Kai Cui for

their technical support and fabrication services. I would also like to acknowledge the funding support of NRC NANO for this research.

Many thanks goes to Pinder for all the help and support on the administrative side of the program.

I am extremely grateful for my family for their unconditional love and support. I get my creativity and patience from my beautiful Maman and my resilience and my passion for nature and art from my lovely Baba. My Mom taught me how to read and write before elementary school and I devoured the first science book series that my parents got me and this sparked my curiosity and passion for science. Thank you for eagerly listening to me talking nonstop about all things science ever since. Your encouragement and kind words have always filled my heart with warmth and love over miles away. My sister, Saba, is the kindest soul I have ever known. Thank you for your encouraging and compassionate words and for all the laughs and chuckles we share just because.

Words cannot express my deep love and appreciation to my amazing husband, best friend and soulmate, Arash. I am extremely grateful for having you in my life. Your nurturing, kindness and unwavering love and support is what kept me going. I look up to you the most, love.

Table of Contents

List of Figures

Abbreviations

BP Bulk Plasmon.

BSE Bethe-Salpeter Equation.

CFEG Cold Field Emission Gun.

CL Cathodoluminescence Light Emission.

CR Cherenkov Radiation.

DFT Density Functional Theory.

DUV Deep Ultra-Violet.

EELS Electron Energy Loss Spectroscopy.

EUV Extreme Ultra-Violet.

eV Electron-Volts.

FFT Fast Fourier Transform.

FIB Focused Ion-Beam Milling.

GIF Gatan Image Filter.

GUI Graphical User Interface.

HSE Heyd-Scuseria-Ernzerhof.

k-EELS Momentum Resolved - EELS.

NSOM Near-Field Scanning Optical Microscopy.

PDOS Photonic Density of States.

q-EELS Momentum Resolved - EELS.

SEM Scanning Electron Microscopy.

SP Surface Plasmon.

SSP Surface Plasmon Polariton.

STEM Scanning Transmission Electron Microscopy.

TEM Transmission Electron Microscopy.

THz Tera-Hertz.

VASP Vienna Ab Initio Simulation Package.

V-EELS Valence-EELS.

ZLP Zero Loss Peak.

Chapter 1

Introduction

1.1 Plasmonics

Plasmonic properties of different materials stem from collective excitations of charged carriers and have lead to unprecedented applications in the field of nanophotonics [1] such as photovoltaic devices [2],[3] medical sensors [4], perfect absorbers [5], [6], lithographic techniques [7], surface enhanced spectroscopy and sensing [8],[9],[10]. There are two separate classes of free electron oscillations in metals. The first class, bulk plasmons, occur at or near the plasma frequency of the metal. It is a resonant phenomenon where collective oscillations of free electrons and light lead to a unique mode, the bulk plasmon. In the second class, the oscillations occur on the surface of the metal, not in the bulk. These are propagating waves with unique electric and magnetic field profiles on the metal's boundary with a dielectric (insulator). These are known as surface plasmon polaritons. Popular material choices in the research community for studying plasmonics include conventional metals (silver, gold, aluminum) as well as highly doped semiconductors (Indium Tin Oxide, Indium Gallium Arsenide).

While the visible, infrared and terahertz (THz) spectral regions have seen considerable advances in terms of light emitting diodes and lasers, the progress in the DUV spectrum has been limited to expensive and bulky plasma sources. There are several

applications in diverse fields such as biological sensing, electronic spectroscopy, UV diffraction and lithography which will benefit from UV photonics. These applications are of interest to researchers in diverse backgrounds ranging from particle physics to medicine. The purpose of this thesis is to explore a new frontier by merging the fields of plasmons and DUV-EUV sources of radiation. DUV plasmonics has remained largely ignored, as most known materials posses metallic properties at lower energy ranges. Identifying materials which have nanophotonic excitations beyond the range of conventional plasmonic materials (e.g noble and Drude metals) that are also suitable for device fabrication, will pave the way towards EUV and DUV electronics. In this research work DUV is defined as a UV radiation with wavelengths between 100 - 300 nm and EUV is defined as a UV radiation with wavelengths between 10 - 100 nm. We use momentum resolved electron energy loss spectroscopy (q-EELS) to characterize optical modes of germanium in order to assess its potential for DUV photonics. This unique technique allows us to map photonic band structure of germanium and demonstrate germanium can support propagating surface plasmons in the DUV range. Further computational efforts are made to design a DUV source employing plasmonic properties of germanium to generate plasmon-assisted DUV radiation. This novel approach for developing DUV sources will solve the long-standing problem to realize an energy efficient and compact radiation source in the DUV energy region of the spectrum, which is compatible with table-top applications making them convenient to use. This innovation builds on our demonstration of the existence of collective excitations of light and matter (surface plasmon polaritons) in thin films of germanium and is less expensive than powerful lasers and x-rays currently used to generate DUV radiation.

In the long-run, access to a miniature light source in the DUV range can open up new probes of matter and also bring germanium photonic technologies (filters, metasurfaces, waveguides, switches, modulators, detectors) to a fundamentally new

part of the electromagnetic spectrum. Our research can lead to an exciting frontier combining fundamental material science and EUV and DUV photonics. Advances in UV photonics benefit many applications in different fields such as biological sensing [11], electronic spectroscopy [12],[13], UV diffraction [14] and lithography [15]. Over the last few decades several technologies have been developed to provide coherent and incoherent electromagnetic radiation in DUV and EUV spectrum. These include synchroton radiation [16] which can be used to produced soft X rays (1-25 nm wavelength). However, the synchroton sources rely on generating ultra-relativistic electrons in large user facilities and are not amenable for use at laboratory scale. A relatively recent approach, which has significantly shrunk the use of electron-driven X-rays, is based on laser-wakefield accelerator [17]. Although this source is smaller in size it involves the use of multiple laser beams to create, heat and drive a plasma. This approach can be prohibitively expensive and complicated for users. Another laser based approach involves high-harmonic generation (HHG) of attosecond pulses using high-intensity femtosecond pulses. Once again, this technology requires considerable expertise with ultra-fast laser systems. Also, the efficiency of the HHG process in terms of power spectral density is quite low. Traditionally excimer laser such as the XeCl lasers operate between 150 nm-200 nm, however they are energy inefficient and not easily scalable. The fundamental issue with development of short wavelength sources is sharp rise in amplified spontaneous emission since the ratio of Einstein's A and B coefficient scales as cube of laser frequency. This makes the lasing process extremely inefficient at short wavelengths. In this thesis, we use a paradigm shift of exploiting relativistic electron-matter interactions to obtain high frequency radiation. We believe this can lead to an important avenue in the future once high efficiencies are obtained.

1.2 Electron Energy Loss Spectroscopy

Advances in optical microscopy techniques have significantly improved spatial resolution yet they are limited by the diffraction limit of the probing light source ($\lambda\backslash 2$). There have been two approaches to achieve higher spatial resolution: 1) using a probing light source with smaller de Broglie wavelength (such as ultraviolet or x-ray microscopy[18]), 2) utilizing near-field probing techniques (such as near-field scanning optical microscopy(NSOM)[19])

The fundamental discovery of the wave-particle duality in early 20th century for particles such as electrons was the cornerstone of developing microscopy techniques based on electrons as the primary source of probing. Electrons having inherently shorter de Broglie wavelength proved to be very useful in surpassing the diffraction limit present in light-based imaging techniques. Electron microscopy has proved to be a disruptive technology in nanophotonics and enables investigation of optical response of materials with unmatched resolution ideal for nanophotonics studies. Electron microscopy configurations are based on analyzing the response of interaction of electron beam with the specimen either through detecting scattered electrons (scanning or transmission electron microscopy (SEM, TEM) set ups) or emitted radiation (cathodoluminescence light emission (CL)) as a result of electron-matter interaction[20].

In addition, electrons possess evanescent electromagnetic field and when swift electrons are passing through thin specimen the large wave-vector component of their EM field couple to high-k modes inside the material. The interaction of the incident electron beam with low energy valence band and collective excitations (plasmons) enables probing excitations far beyond the light cone. Note that free space light cannot probe these high-k modes due to the momentum mismatch of these high-k modes

with light, thus making electrons a unique tool to probe these excitations [21].

STEM-EELS is scanning mode electron microscopy and provides subnanometer spatial resolution on the 1-5 nm scale [22],[23]. EELS provides information on the matter excitations such as bulk plasmons and surface plasmons in the material. Spatial mapping is widely used in the research community but the unique advantage of q-EELS is that q-EELS provides information on momentum-energy dispersion relation of such excitations not obtainable through conventional EELS or STEM-EELS. As swift relativistic electrons undergo energy loss and momentum transfer, it makes q-EELS a unique tool in nanophotonics with unmatched ability to provide information on dispersive optical modes of materials. Using q-EELS as the primary tool to investigate optical response of materials gives insight to dispersive properties of surface plasmon excitations, their group velocities as well as deep subwavelength properties of materials. In this thesis, we exploit it to probe material platform to design optical elements in the emerging field of UV-plasmonics [24],[25],[26],[27].

1.3 Thesis Overview

The thesis is organized as follows. Chapter 2 gives an introduction to the unique technique of momentum-resolved electron energy loss spectroscopy. While the instrumentation for STEM-EELS is widely available around the world in many facilities, this thesis focuses on the momentum-resolution within EELS. This instrumentation coupled with theoretical expertise is available only in a handful of facilities around the world providing a unique foundation for this thesis. Chapter 2 provides an overview of this unique experimental system.

Chapter 3 presents the major contribution in this thesis where deep ultra violet plasmons were demonstrated experimentally in the semiconductor Germanium. Mul-

tiple challenges were overcome to first isolate a free thin film of Germanium to avoid substrate effects. Secondly, DUV plasmons were isolated using momentum-resolved electron energy loss spectroscopy. A theoretical framework was developed in collaboration with theorists to verify the experimental results. Finally, a new experimental device set-up was proposed for building DUV sources of radiation. The work in this chapter can lay the foundation for radiation sources in spectral ranges where conventional photonic sources are not available.

In Chapter 4, we experimentally prove the stability and high temperature properties of plasmons in silicon. We choose the semiconductor system of silicon since it is widely used in the field of photonic crystals, silicon photonics, thermophotovoltaics and nanoscale heat transport engineering. Using a unique temperature dependent q-EELS set-up, we map the plasmons at various temperatures. We show the presence of flat dispersionless bulk plasmons, surface plasmon polaritons as well as Cherenkov radiation of the relativistic electron moving through the silicon sample. An important outcome of this experiment is the stable nature of plasmons at high temperatures showing the potential for applications such as high efficiency, high power DUV sources.

Chapter 2

Momentum-Resolved Electron Energy Loss Spectroscopy

Here we provide an overview of plasmonic applications and momentum-resolved energy loss spectroscopy.

2.1 Plasmonics and its Applications

A significant challenge in characterizing and developing DUV and EUV sources is the absence of optical elements which can be used to develop optical systems. Dielectric materials such as fused silica become increasingly absorptive at shorter wavelengths. Consequently, it is not possible to obtain commercially, photonic elements such as lenses and polarizers, below wavelengths of 180 nm, which serve as building blocks for optical systems.

An important aspect of the development of EUV and DUV sources is investigation and characterization of materials suitable for developing DUV and EUV photonics. Identification of such materials will allow us to refine our preliminary designs and to design geometrical configurations and multi-layered structures for increasingly efficient photonic devices and sources.

2.2 Momentum - Resolved Electron Energy Loss Spectroscopy

Momentum-resolved electron energy loss spectroscopy (q-EELS) is a variation of electron energy loss spectroscopy (EELS) [28] performed in a transmission electron microscope (TEM) [29]. Here, we are concerned with q-EELS in a TEM, as applicable to the valence region of EELS (V-EELS). V-EELS refers roughly as the region from zero-loss peak (ZLP) to the bulk plasmon excitation, of EELS spectra where the EUV and DUV exciations occur. In practise, the corresponding energy loss region spans from a few electron-volts (eV) for optical excitations in the visible region to bulk plasmon excitations in the order of 16 eV in Si or about 35 eV in amorphous carbon.

An electron in a TEM is accelerated to a few hundreds of keV, acquiring speed of 0.5 to 0.7 speed of light. Unlike light, a fast electron can interact with excitations in the material that are outside the dipole region outside of the light cone[20]. q-EELS then records both the amount of energy transferred to the sample, the energy loss, as in conventional EEL spectroscopy. In q-EELS the momentum transfer from the fast electron to the excitations within the sample is additionally recorded, forming a two dimensional (2D) map of energy loss and momentum transfer. The fact that a 2D map of energy and momentum transfer is recorded allows us to link the spectral features to excitations in the sample, and study their dispersion relations. This was demonstrated in our lab earlier[30] for a slab of finite thickness, also linking the q-EELS spectral features to the photonic density of states (PDOS)[31]. The experimental dispersion relations in turn allow to unambiguously determine the origin of the spectral features, such as Cerenkov radiation (CR), surface plasmon polaritons (SPP), bulk plasmons (BP) and interband transitions.

The electron source in the Hitachi HF-3300 TEM is a cold field emission gun

(CFEG) which generates electron beams of high brightness and coherence [32] compared to thermionic and Schottky electron beam sources [32]. Electrons are emitted from a very sharp tungsten tip, where a strong electric field is applied to it to accelerate electrons to energies of the order of 100 keV to 1 MeV [33]. The system operates under high vacuum to avoid sample contamination. The relativistic high energy electrons (300 keV, 0.78c) pass through an array of electromagnetic lenses within the TEM column under high vacuum [34], where a magnified image is formed of a very thin sample (Fig. 2.1).

q-EELS can be applied to both valence region, as discussed in this work and to core loss region. When applied to core loss region, q-EELS can be used to study, for example, bonding anisotropy in materials [28]. In the core loss region, the scattering vector of interest is comparable to the spatial frequencies of atomic lattice, in the order of 1 to 10 nm^{-1}, with an angular resolution of at least $\frac{1}{20}$ of the studied range. The q-EELS applied to core loss region is easily accessible as the microscope settings are identical to those used for selected area diffraction and the incident electron beam convergence angle in the order of 0.1 to 1 mrad can be utilized. This compares to the requirement for sub 10 μrad convergence angle and camera length between about 30 and 100 m needed for V-EELS, as discussed below.

Momentum-resolved EELS is a uniquely powerful technique for probing high-energy states which are inaccessible by photon sources. In this technique, the evanescent field of a free electron couples with a photonic mode of the material. This coupling leads to energy loss in the electron and momentum transfer from the electron. Simultaneous information on energy and momentum transfer from the free electron provides deeper insight into the nature of the material under investigation. Furthermore, q-EELS can be used to probe energy loss and momentum transfer over a large energy range, ranging between 1 to several hundred electron-volts.

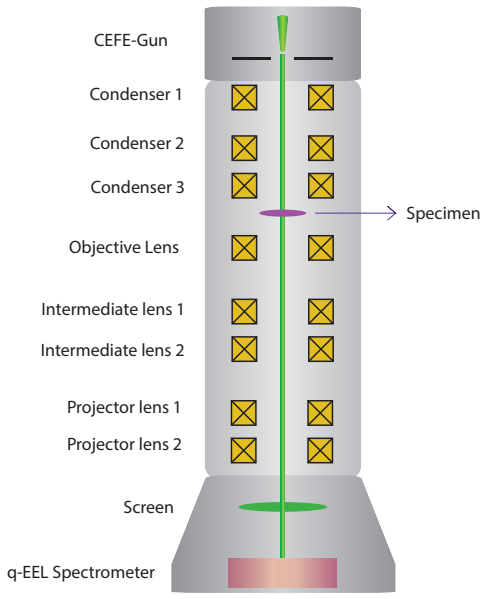

Figure 2.1: **TEM schematic.** Cross section view of the Hitachi HF-3300 TEM, equipped with cold field emission gun (CFEG) to generate coherent beam of electrons. High energy electron beam (300 keV) is aligned through a complex system of electron lenses to produce high resolution image or diffraction pattern of the thin specimen.

The major achievement of this thesis is the experimental identification of DUV and EUV properties of semiconducting materials using a unique probe: q-EELS. There are unique advantages to exploiting electron beams for studying EUV and DUV light-matter interaction since these energy ranges are beyond the reach of traditional optical sources. We now describe the details of the experimental set-up which requires ultra-sensitive calibration and control over relativistic electron beams to provide quantitative dispersion data. One important advantage of high energy electrons are their small wave equivalent de-Broglie wavelength (in the order of a few pm). Thus employing electrons in imaging would significantly reduce the resolution limit to sub-nanometer accuracy which can provide atomic resolution imaging. However, in this work we are interested in momentum resolution so the beam size is made larger in real space to achieve higher accuracy in momentum space.

These electron lenses focus the electron beam to form a magnified image (concep-

tually similar to convex lenses in the visible light microscopes). The condenser lenses demagnify the electron source to form a small probe onto the specimen for added resolution. The objective lens forms the first intermediate image and the first diffraction pattern. The diffraction lenses below the objective lens could then focus on either the image or the diffraction pattern by changing the focal length of the lenses through adjusting the strength of the magnetic lenses. The final image or diffraction pattern is viewed on the fluorescent screen or the CCD camera at the bottom of the TEM column.

Electron lenses deflect off-axis electrons more strongly, introducing spherical aberration to the image formed, meaning a point would be imaged rather into a disk [34]. The spherical aberration limits the resolution of the microscope greatly. Multipole corrector lenses can be used in addition to correct spherical aberration and astigmatism by introducing additional electric field to correct lens defects caused by inhomogeneity of the magnetic field. The resolution of the electron beam and quality of imaging is limited by various elements like electron source, imperfect magnetic lenses, settings of corrector lenses and beam alignment. These factors were optimized during the experimental calibration stage to collect data on Germanium.

The electrons are scattered as they pass through the sample. They transfer some of their energy and momentum to various excitation modes of the sample. The scattered electrons are then collected and mapped according to their energy and momentum loss (Fig. 2.2). The crucial detection system that allows this is the Gatan Image Filter (GIF). An EELS slit selects electrons scattered along the specific momentum k_x to enter the spectrometer. The spectrometer is positioned to exploit the diffraction pattern formed on the back focal plane as an object. Electrons undergo momentum transfer and are scattered at an angle $\theta(\mu rad)$ and electrons of different energies are separated by electromagnetic lenses at the spectroscope and are finally projected onto

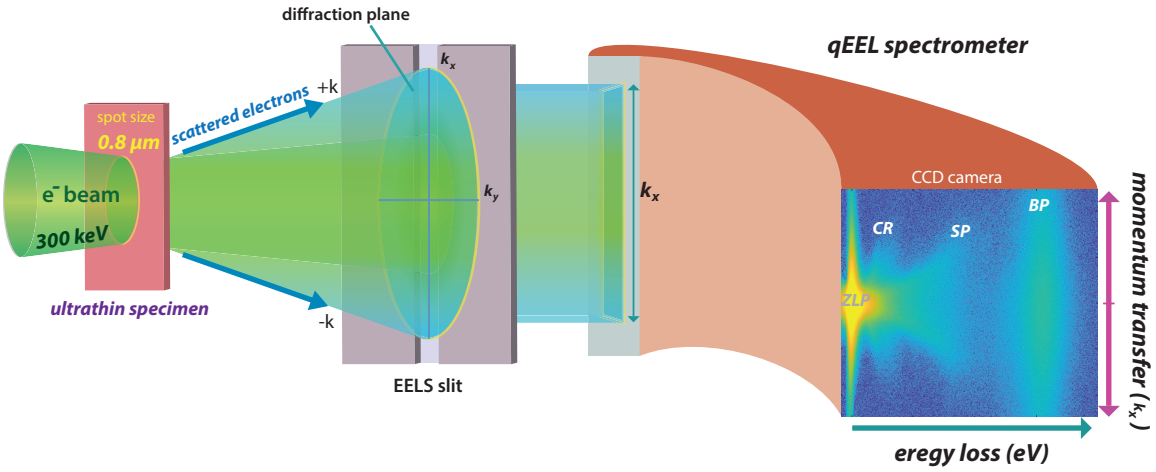

Figure 2.2: **q-EELS schematic.** A transmission electron microscope (TEM) is used to generate an electron beam with energy of 300 keV. In q-EELS these electrons undergo energy loss and momentum transfer when interacting with the nanophotonic excitation modes of the thin sample. High dispersion of q-EELS tool allows energy resolution with high dynamic range and good sensitivity.

the CCD camera. This image on the CCD strikingly shows the energy-momentum dispersion of the optical modes inside the material.

The q-EELS experiment requires a complex system of hardware and software to operate and communicate together, including the TEM and the spectrometer. Maestro [35] is a centralized instrument control system and is based on MATLAB (Fig. 2.3). The experimental setup is fully controlled by a single PC through Maestro and it allows to record the many experimental parameters to access later for data interpretation purposes or loading optical parameters to regenerate the data acquisition conditions. The image acquisition is an automated process of multiple exposures and alignment of acquired data to create a final image, which if it were done manually it would take tremendous amount of labour hours, and it is performed through a Graphical User Interface (GUI) controlled by Maestro.

Theoretical modeling of the energy loss spectra is associated with photonic excitations in thin materials [23]. The dielectric approach with considering retardation

effects provides a complete description of the electron energy loss probability function correspondent to the photonic excitation cross section [22].

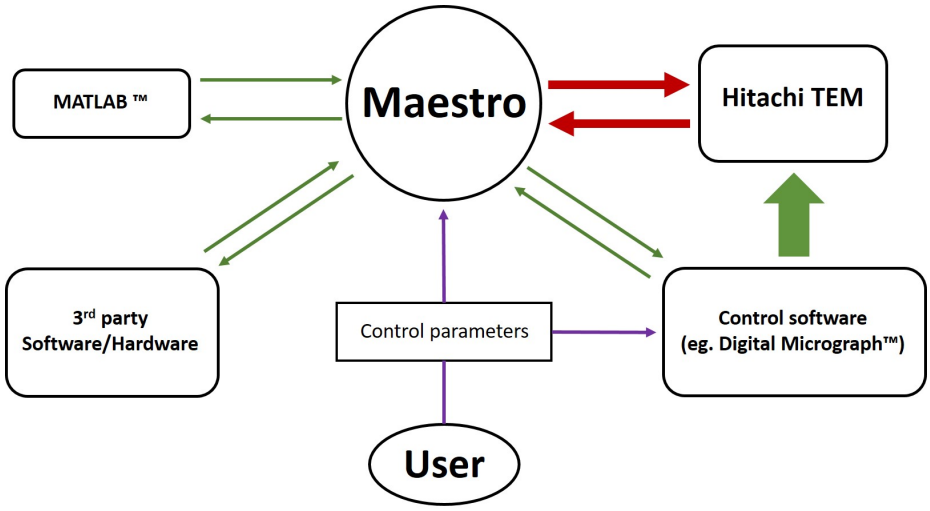

Figure 2.3: **TEM communication layout.** Communication layout of the TEM controlled by MATLAB based centralized control system of Maestro.

We note that q-EELS requires a different setup of the TEM compared to STEM-EELS techniques. For this thesis, q-EELS was performed using a Hitachi HF-3300 TEM/STEM with a cold field emission gun (CFEG) and a Gatan Image Filter (GIF) Tridiem^{TM} as well as the MAESTRO central computer control system. The TEM operation in q-EELS uses a parallel electron beam (300 keV incident energy), different from the point like probe of STEM-EELS with a highly convergent beam. This allows us to map q-space dispersion of the excitations. Relativistic electrons at normal incidence pass through the sample and are scattered simultaneously with a momentum transfer (Δq) as well as energy transfer ($\Delta E = \omega$) mapping directly to the momentum and energy of excitations in the sample with resolutions of ≈ 0.35 μrad and ≈ 0.30 eV, respectively down to ≈ 1.2 eV until the zero loss peak tail. A specified range of scattering angles (corresponding to transferred momentum q) is selected with an EELS slit in the diffraction plane and the high electron energies are dispersed using the EEL spectrometer. The q-EELS experiment was performed in diffraction mode

with about 30 meter camera length and the sample was illuminated with a 0.8 µm diameter probe. The GIF was aligned using a series of energy selecting slits ranging from 10 eV to 2 eV and tuned to have nonisochromaticity to 1^{st} and 2^{nd} order below 0.05 eV and 0.43 eV, respectively. Although the total GIF alignment was performed (including tuning for image distortions, achromaticity, and magnification), no energy selecting slit was used during the q-EELS acquisition. The parallel illumination allows for the entire q-EELS energy-momentum map image for each sample to be recorded using a 1 second acquisition time integrated over 5 images in the GIF spectroscopy mode.

Chapter 3

Deep Ultra-Violet Plasmonics: Exploiting Momentum-Resolved Electron Energy Loss Spectroscopy to Probe Germanium

3.1 Introduction

The plasmonic properties of materials have found a number of applications in the development of photovoltaic devices [2], medical sensors [4], perfect absorbers [5, 6], lithographic techniques [7], surface enhanced spectroscopy and sensing [8–10]. Obtaining the plasmonic properties of different materials across the electromagnetic (EM) spectrum is of great interest for all such nanophotonic applications [1]. Plasmons can be observed in graphene in the terahertz regime [36], highly doped III-V semiconductors in the infrared range [37], metallic systems such as copper (Cu) in the visible [38], and heavy metals such as magnesium (Mg) and gallium (Ga) in the ultraviolet region [39]. Achieving plasmonic properties at much higher energies is a new frontier to design devices in the deep ultraviolet (DUV) regime.

New light sources operating in the extreme ultraviolet (EUV) and deep ultraviolet spectral regions (DUV) have several potential scientific and industrial applications. DUV and EUV sources are extremely important in semiconductor photolithography

techniques. The most popular technique is the immersion lithography [40] which employs excimer laser sources of wavelength 193 nm. Currently, the immersion lithography has been succeeded by EUV lithography through laser-produced plasma sources [41]. The state of art for lithography is at 13.5 nm, however currently a major interest exists in the development of DUV sources for next generation longer wavelength reticles and wafers [42]. DUV sources also have huge relevance in designing helical drilling systems [43], protein structural analysis [44], and angle-resolved photo-emission spectroscopy [45].

In this research work, we have experimentally explored the plasmonic properties of germanium (Ge) in the DUV regime (Fig. 3.1). We show that Ge supports surface plasmon polaritons (SPP) in the DUV region with its surface plasmon resonance more than twice that of aluminum, a typical material of choice to construct UV devices. One can employ DUV plasmons in Ge to construct DUV waveguides, metamaterials, and other devices that are currently not possible with other conventional plasmonic materials. Germanium is a technologically important material thanks to its semiconducting properties at the infrared wavelengths. Counter-intuitively, here we show that Ge acts like a Drude-type metal in the DUV region.

We probe the plasmonic properties of germanium using relativistic electrons through momentum resolved electron energy loss spectroscopy (q-EELS). Unlike the traditional electron energy loss techniques [46], in this work both the energy and momentum dispersion of the plasmons are mapped simultaneously [30, 31]. This allows us to obtain the plasmonic behavior and the corresponding photonic band spectrum in thin Ge single crystal slabs even as small as 60 nm. The measured photonic band spectrum shows an excellent agreement with the macroscopic electrodynamics electron energy loss theory. Furthermore, we explain the dielectric behavior of DUV plasmons in Ge through first-principles density functional theory (DFT) calculations. Finally, we

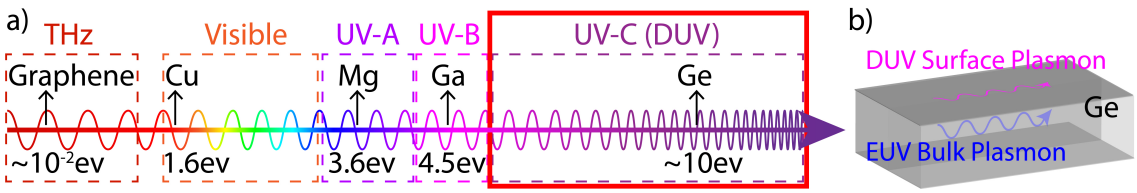

Figure 3.1: **DUV plasmonics across electromagnetic spectrum.** a) Comparison of surface plasmon frequency in different material systems across the electromagnetic spectrum. b) Schematic display of bulk and surface plasmons in Germanium.

numerically simulate a Smith-Purcell radiation source (with a wavelength resonance close to 145 nm) in the DUV regime by employing SPP in Ge.

3.2 DUV Plasmons in Germanium Measured With q-EELS

The DUV plasmonic properties of germanium are measured with relativistic electrons and q-EELS setup in a transmission electron microscope (TEM). Traditional electron energy loss spectroscopy techniques account only for the amount of energy loss of the electron. In q-EELS, the momentum loss information is also obtained by measuring the scattering angle (θ) of the electron after passing through the sample. The amount of energy and momentum carried away by the excitations within the sample directly corresponds to the energy and momentum lost by the incident electron. Thus, using q-EELS one can clearly map the photon/polariton band structure [31] and identify photonic excitations such as Cherenkov radiation (CR), waveguide modes, surface plasmon (SP) and bulk plasmon (BP).

The samples were prepared via focused ion beam milling (FIB) and mounted on a TEM grid to create free-standing ($10\,\mu\text{m} \times 5\,\mu\text{m}$) slabs with thickness 60 nm, 100 nm and 200 nm. The focused ion beam milling is conducted through a 40 keV Ga^+ ion beam in a Hitachi NB5000 dual beam instrument, and polished using a 5 keV Ga^+ ion beam to reduce amorphous layer. This is important as we try to observe SPP, as

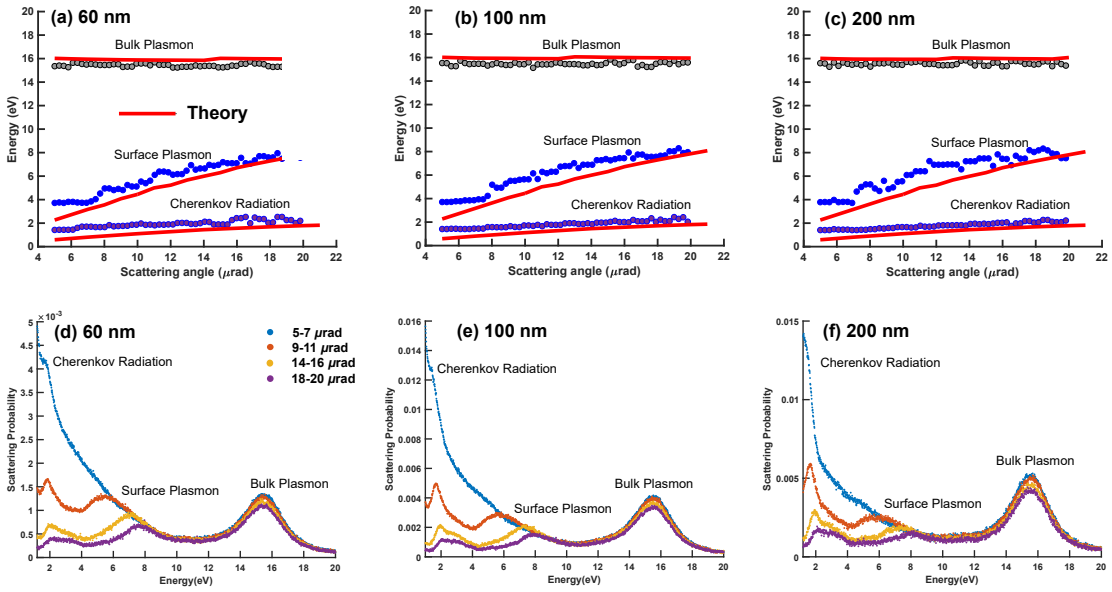

Figure 3.2: **q-EELS measurements for germanium.** (a), (b), (c) Photonic band structure of thin germanium samples of thicknesses 60 nm, 100 nm and 200 nm are measured using q-EELS. The dispersionless BP is observed at $\sim$ 16 eV, the SPP lies at the DUV energy range (4-10 eV) and the CR is observed at 2-4 eV. The solid lines represent the energy-momentum dispersion of the scattered electrons obtained using macroscopic electrodynamics calculations. (d), (e), (f) The electron scattering probability for all three exciations as measured by q-EELS integrated over several scattering angle intervals are plotted as a function of energy for the 60, 100, and 200 nm thin germanium slabs, respectively. A blue-shift is observed for the peak of the surface plasmon with increase in scattering angle for all three samples, whereas no such shift is observed for the bulk plasmon peak.

the surface needs to be free of Ga^+ damage as much as possible.

In Figs. 3.2(a)–(c), we have shown the photonic band spectrum measured using q-EELS for the free standing Ge samples of thicknesses 60 nm, 100 nm and 200 nm, respectively. A flat-band is observed at 16 eV without any dispersion in all three samples. This flat-band is attributed to the BP excitation of germanium. Bulk plasmons occur when $\varepsilon_{\mathrm{Ge}} \to 0$, which is well into the EUV regime (See Fig. 3.1). We note that such longitudinal BP oscillations occur at such high energies even in other materials

such as aluminum and silicon [30].

The highly dispersive bands observed between $\approx 4 - 10\,\mathrm{eV}$ in Figs. 3.2(a)–(c) are the surface plasmon polariton excitations of Ge in the DUV regime. Note that $\omega_{\mathrm{sp}} = \omega_{\mathrm{p}}/\sqrt{2} \approx 11.3\,\mathrm{eV}$, which indicates that Ge is a Drude-like metal in the DUV. This is in stark contrast with the semiconducting properties of the Ge observed at visible and infrared wavelengths. The highly dispersive nature of SPP bands are further evident in Figs. 3.2(d)–(f), where we have plotted the scattering probability as a function of energy, obtained within several intervals of scattering angles. We observe a blue-shift in the SPP peak with increase in scattering angle for all three samples, whereas no such shift is observed for the BP peak. In the following, through DFT calculations we explain that the metallic nature of Ge in DUV regime is due to the weak interband transitions between valence and conduction bands, which creates unbound valence plasmons that can support SPP excitations.

Band structure of Germanium is calculated using HSE06 hybrid functional [48] along W-L-Γ-X-W points (see Fig. 3.3(a)) in the Vienna Ab Initio Simulation Package (VASP) [49]. Hybrid functional approximates the exchange correlation functional by separating electron interaction into long-range and short-range part in the exchange energy. In the DUV region, the interband transition between valence band and conduction band is very weak and the electrons in valence band behave like free electrons which leads to the plasmonic behavior of germanium in the DUV region.

Dielectric function of germanium shown in Fig. 3.3(b) is calculated using GW_0 & Bethe-Salpeter Equation (BSE) in VASP. GW_0 & BSE takes the excitonic effects into consideration on top of GW_0 results for the electron energy. In the DUV regime, electron-hole pairs are not tightly bound and the dielectric function reduces to a simpler form similar to Drude model with $\mathrm{Re}(\varepsilon) < 0$. At high frequencies, valence

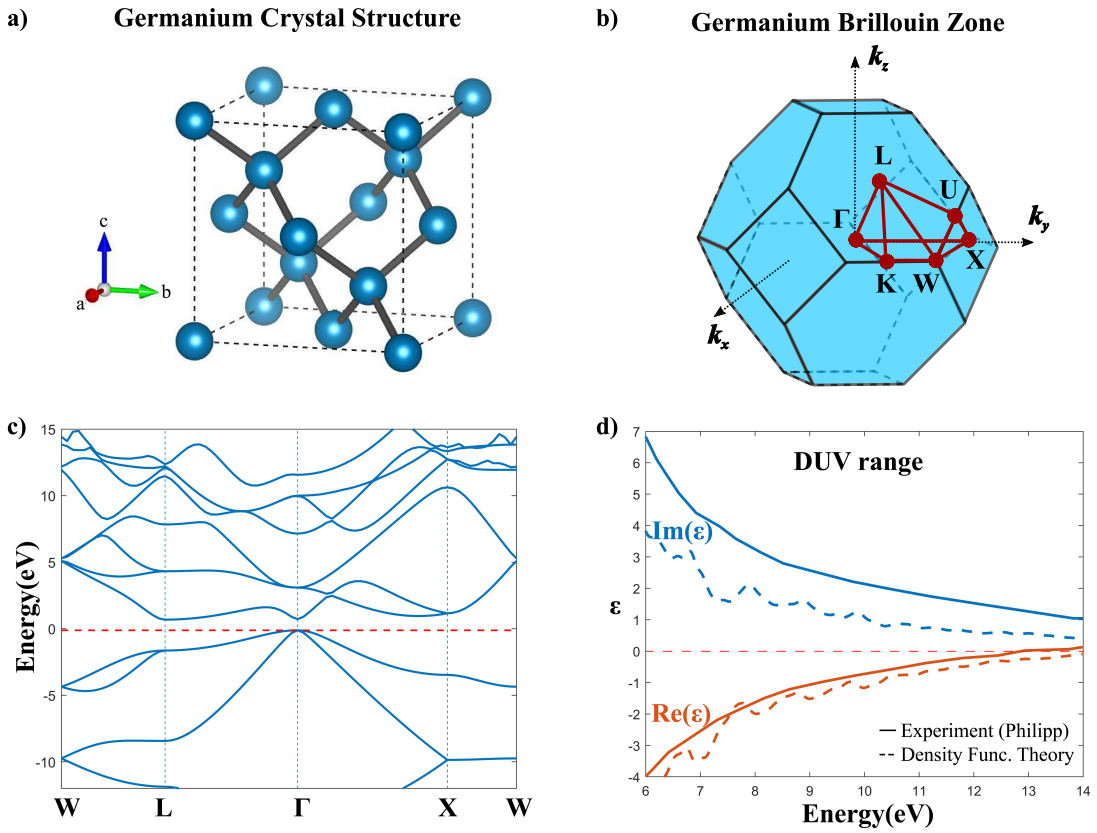

Figure 3.3: **Band structure calculations of germanium.** (a) The face-centered diamond-cubic crystal structure of germanium is shown. (b) The first Brillouin zone and the high symmetry points of the germanium crystal are displayed. (c) Electronic band structure of germanium obtained using density functional theory calculations is plotted. (d) Experimental [47] and density functional theory calculation values for the permittivity of germanium are compared. Plot shows the metallic character of germanium in the DUV ($\varepsilon < 0$) in the 6–12 eV (103–207 nm) range.

electrons behave as collective oscillations instead of undergoing interband transition. In Ge, due to exhaustion of f-sum rule [47] in the DUV region, valance band electrons behave effectively like unbound free electrons and contribute to the observed metallic behavior. For frequencies below the transition frequency between d-band and conduction bands, coupling between bounded d-band electrons and unbounded valance electrons will not disturb the Drude-like optical response [47].

Further, we compare our experimental data with the simulations of the macroscopic electrodynamics electron energy loss function [22] in Ge for electrons normally

incident on the sample. In Fig. 3.2(a)-(c) we see that the measured data show a strong match with the theoretical calculations (shown in solid lines).

Finally, we observe a low energy branch in the visible range (1.5–2.5 eV) in Fig. 3.2. Through electron energy loss function theory, we recognize that this low energy branch is the visible CR in germanium. When an electron passes through a medium with a velocity greater than the phase velocity of light in the medium, it generates the CR radiation. Such CR radiation has been observed previously in energy loss experiments [27, 50, 51], metamaterials [52, 53], and even in two-dimensional materials [54, 55]. In dielectrics, CR occurs if the electron velocity is larger than the phase velocity in the medium ($v \geq c/\sqrt{\varepsilon}$). The threshold electron velocity for the relativistic electrons used in our experiment is achieved when $\varepsilon \geq 1.64$. In our q-EELS experiment, the incident electron beam energy is set at 300 keV ($v \approx 0.79c$), which is above the CR radiation threshold.

3.3 DUV Radiation Source in Germanium

Light-matter interactions mediated through periodic structures have been employed often in stimulating scientific and technological advancements. A worthy objective premised upon the same is to design alternative sources of light. One such phenomenon dependent upon the periodicity of the medium is the Smith-Purcell effect which was first experimentally demonstrated in 1953 [56]. It was observed that the charged particles moving close to a periodic structure at a constant velocity emit electromagnetic waves. In this section, we numerically simulate a DUV radiation source in Ge based on the Smith-Purcell effect.

In a periodic grating structure, non-radiating evanescent surface modes exist near the surface. An electron beam moving above the grating interacts with these evanes-

cent surface modes. As a result, Smith-Purcell radiation is created during this transient process[57]. Smith-Purcell radiation is typically observed in metallic grating structures. For a perfect electric conductor (PEC) grating, the wavelength of the Smith-Purcell radiation is given by [57] $\lambda = (a/g)\,(\cos\theta - 1/\beta)$, where a is the periodicity of the surface and g is the diffraction order (a negative integer), $\beta = v/c$, and θ is the angle of propagation of the emitted electromagnetic wave relative to the initial direction of particle motion.

Smith - Purcell radiation phenomenon can be alternatively understood through the method of image charges. When an electron is moving above a periodic grating structure, the distance between the electron and its image charge has a periodic variation [58]. The resulting oscillating dipole moment created by the electron and its image charge emits the electromagnetic radiation [59]. However, if we pass an electron beam through a hole grating structure (Fig. 3.4(a)) instead of the electron beam above a periodic grating structure, the number of dipole oscillations is quadrupled, and thereby enhancing the intensity of the radiation in the far-field regime.

We can utilize the metallic behavior of Ge in the DUV region to design Ge based free electron laser source. We propose a hole grating structure made up of Ge as shown in Fig. 3.4(a). The hole grating structure is constructed to significantly enhance the Smith-Purcell radiation.

To confirm the existence of Smith-Purcell radiation from the Ge based periodic structure, we simulate this source by particle-in-cell (PIC) method in CST Studio Suite[60]. In this simulation, a is chosen to be 35 nm with grating hole size 20×20 nm. Electrons pass through the grating structure with a kinetic energy of 20 keV. Given an electron beam propagating through the grating along the positive x-axis, we analyze the transient and frequency response of the far-field radiation pattern at different

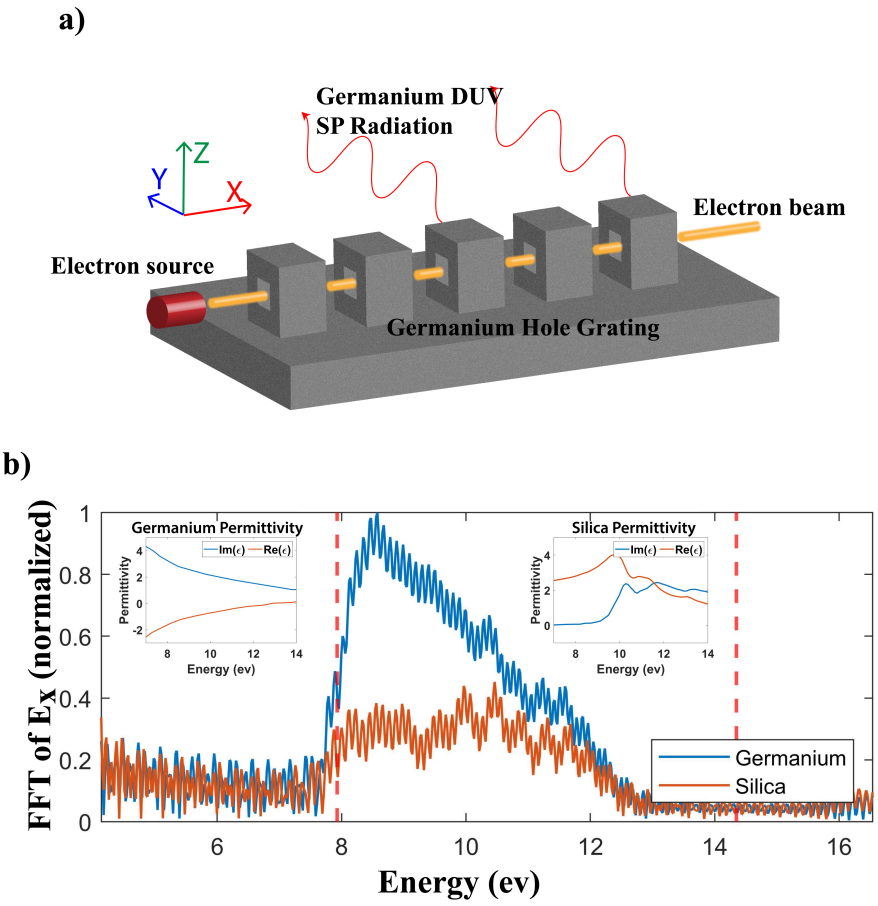

Figure 3.4: **DUV light source design.** (a) The schematic diagram depicts the Ge hole grating structure for generating the Smith-Purcell radiation. (b) The fast Fourier transform (FFT) of the radiated E_x field component is plotted as a function of frequency for Ge and silica. Smith-Purcell radiation for the hole grating structure is simulated by PIC method in CST [60]. Radiation peak around 8.6 eV (145 nm) is observed in the spectra of E_x for the Ge grating structure. Germanium has a distinctive radiation peak due to its metallic nature in the DUV regime, whereas such a peak is absent in silica. Inset shows the difference in the behavior of dielectric function for both Ge [47] and silica [61] in the DUV regime.

observation points. The resulting Smith-Purcell radiation component E_x is plotted as a function of frequency in in Fig. 3.4(b).

From the spectra of E_x, we find a broad peak with its center close to 8.6 eV (145 nm). Position of this peak matches with the frequency range defined by spectral order $g = -1$ (shown by the region between two dashed vertical red lines in Fig. 3.4(b)). Origin of this phenomenon is the metallic behavior of Ge in the DUV region. In order to show the contrast, we also simulated the radiation from the same hole grating structure made with silica. The result is shown by the orange curve Fig. 3.4(b). We find that the real part of silica's permittivity is positive in this frequency range and as a result, radiation peak in the DUV range is not distinct. Whereas, Ge has negative values of the real part of permittivity in the same range (see inset in Fig. 3.4(b)), as a result we obtain a radiation peak close to 8.6 eV.

It should be noted that the radiation created by a continuous electron beam is not coherent, and does not have a unique direction. We can easily solve these problems by instead injecting groups of electrons in intervals. The idea is to shape the electrons into groups with a required frequency and pass it through the hole grating structure to create a super-radiant emission [58, 62]. With this extension, by using the proposed grating structure made from Ge one can design a coherent unidirectional DUV laser source. This idea will be discussed further in a future publication.

Chapter 4

Probing Plasmonic Excitations at High Temperatures in Silicon

4.1 Introduction

Silicon is the most prominent material of choice in the semiconductor industry and is well known for its semiconducting and dielectric properties. Being compatible with materials used in microelectronics alongside with rapid advances in nanofabrication techniques paves the way to the extensive use of silicon in modern technology. Silicon plasmonics applications were introduced in the research community by heavily doping silicon to achieve metallic properties in the near-infrared spectral range for photodetection, sensing and enhanced absorption in solar cells. Recently it has been pointed out that silicon can be useful in a new application: DUV and EUV sources, since it can support surface plasmon excitations in the EUV spectral range [30] . This is in the contrast to the doping based approach for silicon to exploit metallic behaviour. This paves the way to UV plasmonics in silicon and future applications in highly compact nanophotonics and lab-on-chip nanostructures.

In this study, we investigate the presence of surface plasmon excitations in silicon at the ultraviolet region at higher temperatures up to 400 °C and their stability under such conditions. The motivation for this study is multiple-fold. In the previous chapter, we explored Germanium plasmons for the first time in DUV and EUV regions and proposed sources of radiation using electron-matter interactions. When these

interactions occur and cause the DUV radiation to emanate from the nanophotonic structure, a large amount of heat is simultaneously generated due to absorption. This will cause a temperature increase and it is unclear whether the plasmonic response will be modified or will be heavily damped at high frequencies. Another important motivation to study the high temperature properties of silicon is for the field of thermophotovoltaics. Silicon is used for photonic crystal based high temperature emitters. The plasmonic properties can enhance the spectral selectivity so it is necessary to study the stability of high temperature plasmons. Finally, the thermal coefficient of expansion and other thermal properties can also be identified using the sensitive nature of the bulk plasmon and surface plasmon resonant frequencies. Thus studying the resonant frequencies as a function of temperature can shed light on intrinsic bulk thermal properties of materials.

4.2 Experimental Results

One important constraint for performing q-EELS is to remove the substrate effects completely. We achieved this using focused ion beam milling and creating 80 nm to 300 nm thick samples of semiconductors. Surface contamination was minimized but can play a role in the variations of the SP peak. Two silicon films of thicknesses 100 nm and 200 nm were fabricated through FIB technique and were mounted on a TEM grid as freestanding ultrathin films. The TEM grid was then transferred to the TEM column on an electrically heated sample holder: the Gatan heating holder. The heating holder was connected to a power supply outside the TEM tool through auxiliary electric connections. This Gatan hot stage controller changes the temperature of the specimen by applying change to the electrical current at a desired rate.

We first conducted room temperature measurements for 100 nm silicon film and 200 nm silicon films. Then unique temperature stages were leveraged to raise the temperature of the samples to 400 °C at 10 °C/min. We let the sample stabilize

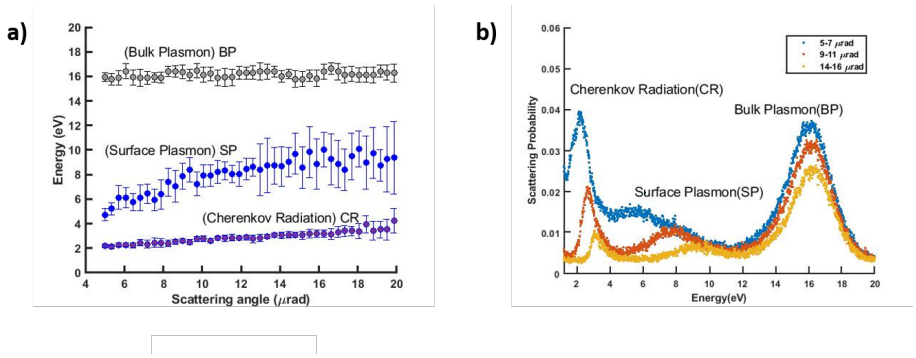

Figure 4.1: **q-EELS measurements,** for 100 nm silicon film at room temperature showing the bulk plasmon, surface plasmon and Cherenkov radiation. (a) Energy-momentum dispersion relation of CR, BP and SP excitations. (b) Integrated energy-loss function over various scattering angles: 5 - 7 μrad, 9 - 11 μrad, 14 - 16 μrad. There is a blue-shift observed in the CR-peak and SP-peak by increasing the scattering angle.

overnight at 400 °C and then q-EELS measurements were performed at 400 °C. Furthermore, we varied the temperature down to room temperature (using the Gatan hot stage controller) while performing q-EELS measurements at fixed temperatures of 300 °C, 200 °C, 100 °C and 23 °C. We allowed the sample to stabilize after each temperature change for several hours.

The key takeaway from the experimental results were the observation of Cherenkov radiation and plasmonic excitations which are robust to high temperature for ultra-thin silicon films. There exists a bulk plasmon excitation which is a dispersionless flat band around 16 eV. There also exists a surface plasmon polariton with characteristic dispersion extending from 4 to 10 eV. Finally in the transparent range, there exists Cherenkov radiation from 2 - 3.5 eV. There is a blue-shift in the surface plasmon peak and Cherenkov radiation peak with increasing scattering angle. We perform a Gaussian fit with MATLAB to calculate SP peak from 1-D plots where electron energy loss in integrated over scattering angles of 9 - 15 μrad. It is seen that SP peak average for 100 nm sample is 8.46 eV while SP peak average for 200 nm sample is 8.05 eV.

Experimental results of the room temperature data for the free-standing silicon

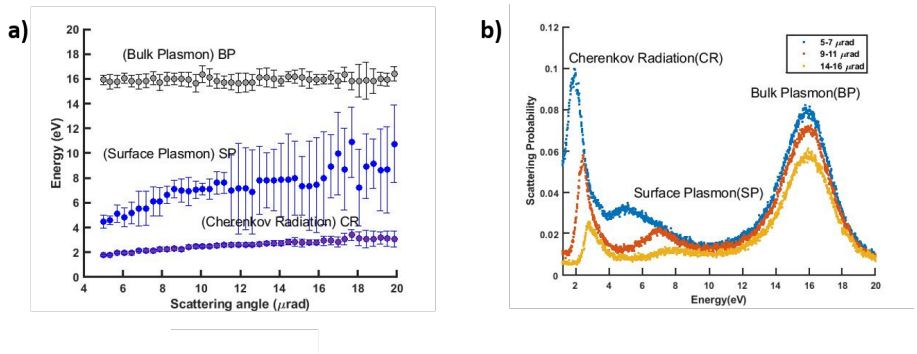

Figure 4.2: **q-EELS measurements,** for 200 nm silicon film at room temperature showing the bulk plasmon, surface plasmon and Cherenkov radiation. This forms our baseline comparison for high temperature measurements.

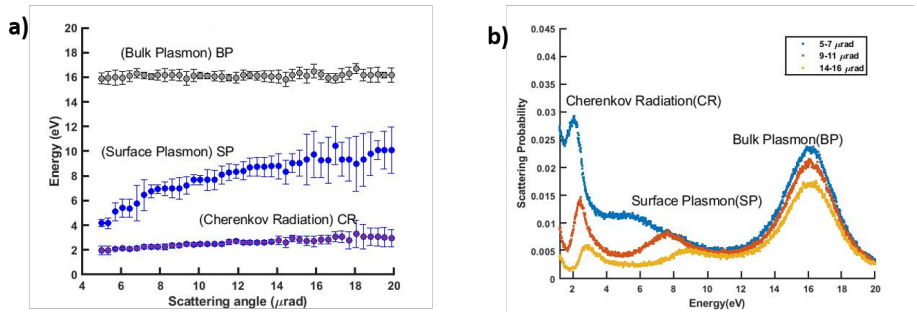

Figure 4.3: **q-EELS measurements,** for 100 nm silicon film at 400 °C.

samples of thicknesses 100 nm and 200 nm are presented in figures 4.1 and 4.2, followed by high-temperature q-EELS data in figures 4.3 and 4.4. Comparing the room temperature data and 400 °C data indicates that the optical modes are stable at higher temperatures both for 100 nm and 200 nm samples. A closer look at the SP dispersion band (4.5) shows that the peak of surface plasmon excitations for the integrated angles of 9 - 15 μrad, is between 7.5 - 8.5 eV. We expected to see larger variations with temperature of the surface plasmon peak but surface contamination and energy resolution could be limiting factors. Recently a high resolution spectrometer has been obtained and future work will focus on isolating the thermal properties through the shift in the resonant peaks.

In addition, we also perform density functional theory calculations (4.8, 4.9) to analyze the response function of silicon and take a closer look at the EUV region

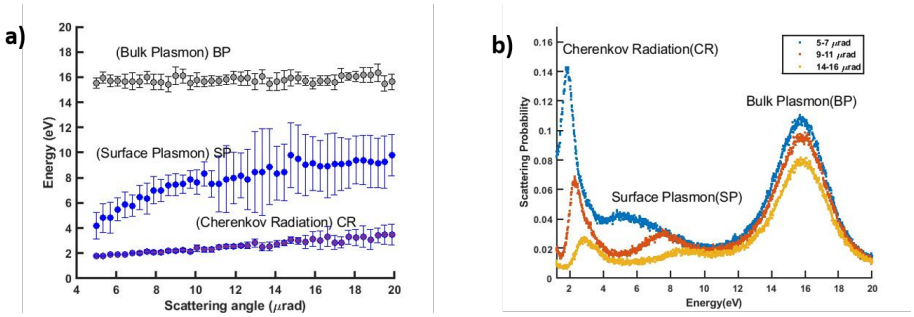

Figure 4.4: **q-EELS measurements,** for 200 nm silicon film at 400 °C.

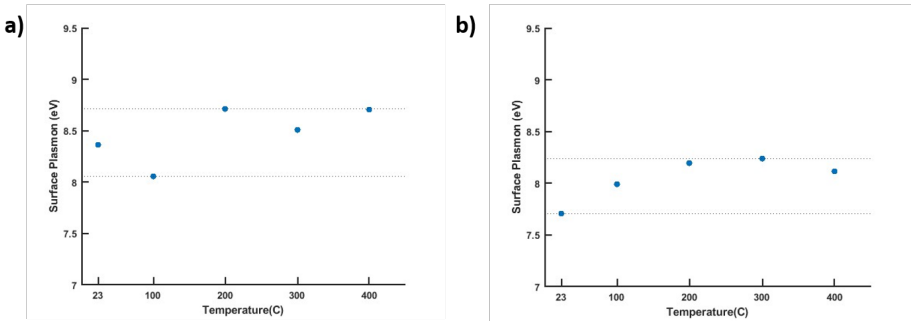

Figure 4.5: **Surface plasmon peak,** for (a)100 nm sample and (b) 200 nm sample with average surface plasmon peak at 8.46 eV and 8.05 eV respectively.

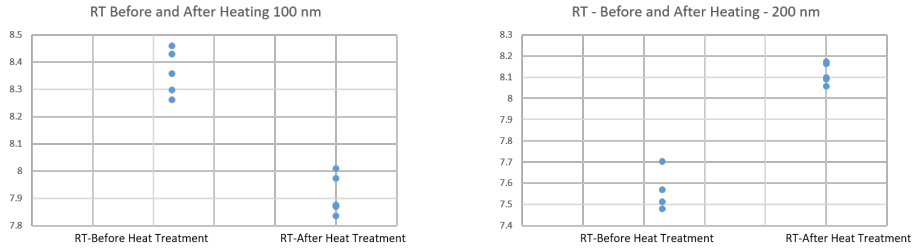

Figure 4.6: **Surface Plasmon Peak at RT,** for the 100 nm and 200 silicon film at RT before heating the sample and after cooling sample from 400 °C down to room temperature.

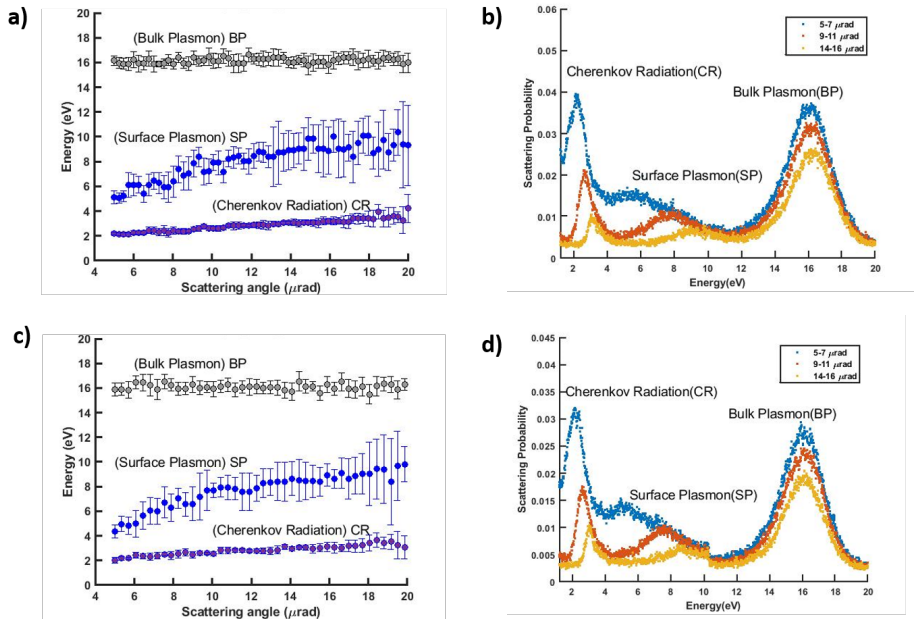

Figure 4.7: **q-EELS measurements at room temperature,** for the 100 nm silicon film (a-b)at RT before heating the sample and (c-d) after cooling sample from 400 °C down to room temperature.

in the dielectric. They are performed by our collaborators with the GW method and Bethe-Salpeter equation. The Ab-initio calculations are performed with the Vienna Ab Initio Simulation Package (VASP). The dielectric function is calculated with the GW + Bethe-Salpeter Equation (BSE) method. We consider the cutoff energy to be 250 eV for the plane-wave-basis set in the calculations. We employ shifted Monkhorst–Pack mesh to sample the Brillouin zone and average over the results to improve the dielectric function. These results show that the exciton nature of the interband transitions plays a key role in matching theory and experiment.

4.3 Conclusion

We have shown the dispersion of bulk plasmons, surface plasmon polaritons and Cherenkov radiation for ultra thin silicon films at both room temperature and elevated temperatures. This is the first study that utilizes q-EELS at high temperatures and thus presents unique data for the research community. In the future using advanced

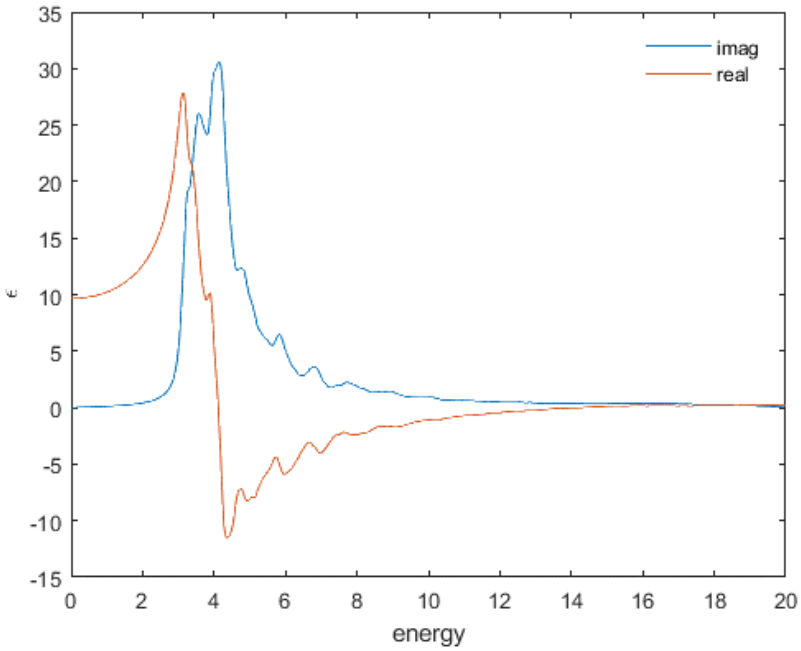

Figure 4.8: **Silicon dielectric function calculation.**

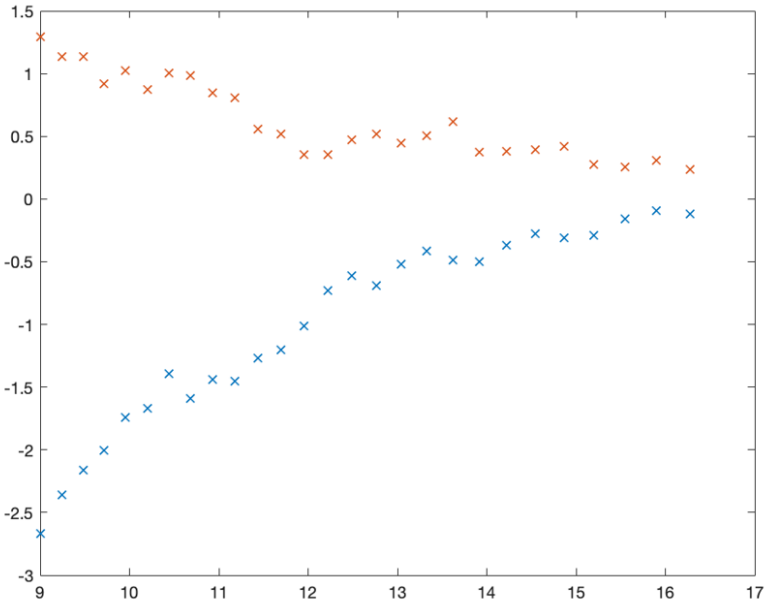

Figure 4.9: **Silicon dielectric function, across the ultraviolet spectrum.**

theoretical analysis and a high resolution spectrometer, it will be possible to analyze the thermal expansion properties of materials using the shift in the surface plasmon peaks. We thus believe our data to be of considerable value to the research community engaged in multiple fields from silicon photonics and thermophotovoltaics to nanoscale thermal properties of matter.

Chapter 5

Conclusions, Recommendations and Future Work

5.1 Conclusion

We have experimentally demonstrated the existence of DUV surface plasmons in germanium with its resonance energy twice as large as those observed in conventional metals such as aluminum. Through q-EELS technique, we could map the plasmonic excitations in Ge (bulk plasmons, surface plasmonics and Cherenkov radiation) up to a large energy and wavevector values that are not possible through traditional electron energy loss spectroscopy techniques. The measured photonic band spectrum has a strong match with the macroscopic electron energy loss theory. We have described the observed metallic behavior of Ge in the DUV region through first-principles density functional theory calculations. Further, we employ the DUV plasmons in Ge to design a DUV radiation source based on the Smith-Purcell radiation phenomena. By passing an electron beam through a Ge hole grating structure, we demonstrated a radiation resonance close to 145 nm. This free electron radiation source has a great potential to be employed in DUV device applications.

5.2 Future Work

In future work, we recommend studying q-EELS of various semiconductor systems to isolate deep ultraviolet and extreme ultraviolet responses. This can lead to a new generation of sources for DUV and EUV lithography. Other important questions are related to how crystal lattice symmetries affect the EELS spectrum. In this current work, we have focused on using crystalline samples which are cut out from commercially available wafers. On the other hand, the role of disorder and amorphous phases have not been explored in detail. The current results help to isolate the role of surface plasmon polaritons as well as bulk plasmons. They occur due to interband transitions in bulk 3D semiconductors in stark contrast to conventional metals. We believe plasmonic confinement effects similar to metallic constituents are possible even with semiconductors. This is due to the low imaginary part of the dielectric constant away from the interband absorption resonance.

Another future direction is related to phonon-polaritons. They are lower energy excitations than plasmon-polaritons but can deflect the incoming electrons. The energy resolution needed to resolve phonon-polaritons is around 100 mev which is very challenging. This is because the zero loss peak in the current experimental set-up is around 1 eV. Phonon polaritons are excitations of optical phonons and light. Acoustic phonons are lower in energy and exhibit weak interaction with electron beams.

In this thesis, we have worked on temperature dependent plasmonic properties. This allows us to understand how plasmons will behave in the high temperature environment which occurs in deep UV sources. By increasing the spectral resolution, we believe it will be possible to study the peak shifts of the bulk plasmons and extract bulk thermal properties of materials.

Bibliography

[1] P. R. West, S. Ishii, G. V. Naik, N. K. Emani, V. M. Shalaev, and A. Boltasseva, "Searching for better plasmonic materials," *Laser & Photonics Reviews*, vol. 4, no. 6, pp. 795–808, 2010.

[2] H. A. Atwater and A. Polman, "Plasmonics for improved photovoltaic devices," *Materials for sustainable energy: a collection of peer-reviewed research and review articles from Nature Publishing Group*, pp. 1–11, 2011.

[3] S Pillai, and M. Green, "Plasmonics for photovoltaic applications," *Solar Energy Materials and Solar Cells*, vol. 94, no. 9, pp. 1481–1486, 2010.

[4] M. I. Stockman, "Nanoplasmonics: The physics behind the applications," *Phys. Today*, vol. 64, no. 2, pp. 39–44, 2011.

[5] N. Liu, M. Mesch, T. Weiss, M. Hentschel, and H. Giessen, "Infrared perfect absorber and its application as plasmonic sensor," *Nano letters*, vol. 10, no. 7, pp. 2342–2348, 2010.

[6] M. Pu *et al.*, "Design principles for infrared wide-angle perfect absorber based on plasmonic structure," *Optics Express*, vol. 19, no. 18, pp. 17 413–17 420, 2011.

[7] A. Kristensen *et al.*, "Plasmonic colour generation," *Nature Reviews Materials*, vol. 2, no. 1, pp. 1–14, 2016.

[8] J. P. Camden, J. A. Dieringer, J. Zhao, and R. P. Van Duyne, "Controlled plasmonic nanostructures for surface-enhanced spectroscopy and sensing," *Accounts of chemical research*, vol. 41, no. 12, pp. 1653–1661, 2008.

[9] A. J. Haes, C. L. Haynes, A. D. McFarland, G. C. Schatz, R. P. Van Duyne, and S. Zou, "Plasmonic materials for surface-enhanced sensing and spectroscopy," *MRS bulletin*, vol. 30, no. 5, pp. 368–375, 2005.

[10] R. F. Aroca, "Plasmon enhanced spectroscopy," *Physical Chemistry Chemical Physics*, vol. 15, no. 15, pp. 5355–5363, 2013.

[11] A Ono, M Kikawada, R Akimoto, W Inami, and Y Kawata, "Fluorescence enhancement with deep-ultraviolet surface plasmon excitation.," *Optics Express*, vol. 21, no. 15, pp. 17 447–17 453, 2013.

[12] A. Bhuiyan, A Satija, S. Naik, and R. Lucht, "Development of two-color laser system for high-resolution polarization spectroscopy measurements of atomic hydrogen," *Optics letters*, vol. 37, no. 17, pp. 3564–3566, 2012.

[13] T. Softley, W. Ernst, L. Tashiro, and R. Zare, "A general purpose xuv laser spectrometer: Some applications to n2, o2 and co2," *Chemical physics*, vol. 116, no. 3, pp. 299–309, 1987.

[14] M. Bargheer, N Zhavoronkov, M Woerner, and T. Elsaesser, "Recent progress in ultrafast x-ray diffraction," *Chemphyschem: a European journal of chemical physics and physical chemistry*, vol. 7, no. 4, pp. 783–792, 2006.

[15] C. Wagner and N. Harned, "Lithography gets extreme," *Nature Photonics*, vol. 4, no. 1, pp. 24–26, 2010.

[16] J Nordgren, G Bray, S Cramm, R Nyholm, J.-E. Rubensson, and N Wassdahl, "Soft x-ray emission spectroscopy using monochromatized synchrotron radiation," *Review of Scientific Instruments*, vol. 60, no. 7, pp. 1690–1696, 1989.

[17] C. Geddes *et al.*, "High-quality electron beams from a laser wakefield accelerator using plasma-channel guiding," *Nature*, vol. 431, no. 7008, pp. 538–541, 2004.

[18] W. Chao, B. D. Harteneck, J. A. Liddle, E. H. Anderson, and D. T. Attwood, "Soft x-ray microscopy at a spatial resolution better than 15 nm," *Nature*, vol. 435, no. 7046, pp. 1210–1213, 2005.

[19] A Hartschuh, H Qian, C Georgi, M Böhmler, and L Novotny, "Tip-enhanced near-field optical microscopy of carbon nanotubes," *Analytical and bioanalytical chemistry*, vol. 394, pp. 1787–1795, 2009.

[20] F. G. De Abajo, "Optical excitations in electron microscopy," *Reviews of modern physics*, vol. 82, no. 1, p. 209, 2010.

[21] R. F. Egerton *et al.*, *Physical principles of electron microscopy*. Springer, 2005, vol. 56.

[22] C. Chen and J Silcox, "Calculations of the electron-energy-loss probability in thin uniaxial crystals at oblique incidence," *Physical Review B*, vol. 20, no. 9, p. 3605, 1979.

[23] F. G. De Abajo and M Kociak, "Probing the photonic local density of states with electron energy loss spectroscopy," *Physical Review Letters*, vol. 100, no. 10, p. 106 804, 2008.

[24] M. Bosman, V. J. Keast, M. Watanabe, A. I. Maaroof, and M. B. Cortie, "Mapping surface plasmons at the nanometre scale with an electron beam," *Nanotechnology*, vol. 18, no. 16, p. 165 505, 2007.

[25] J. Nelayah *et al.*, "Mapping surface plasmons on a single metallic nanoparticle," *Nature Physics*, vol. 3, no. 5, pp. 348–353, 2007.

[26] C. Colliex, M. Kociak, and O. Stéphan, "Electron energy loss spectroscopy imaging of surface plasmons at the nanometer scale," *Ultramicroscopy*, vol. 162, A1–A24, 2016.

[27] R. F. Egerton, *Electron energy-loss spectroscopy in the electron microscope*. Springer Science & Business Media, 2011.

[28] R. F. Egerton, *Electron Energy Loss Spectroscopy in Electron Microscope*. 2011.

[29] H. Kohl and L. Reimer, *Transmission electron microscopy: Physics of Image Formation*. Springer, 2008.

[30] P. Shekhar *et al.*, "Extreme ultraviolet plasmonics and cherenkov radiation in silicon," *Optica*, vol. 5, no. 12, pp. 1590–1596, 2018.

[31] P. Shekhar, M. Malac, V. Gaind, N. Dalili, A. Meldrum, and Z. Jacob, "Momentum-resolved electron energy loss spectroscopy for mapping the photonic density of states," *Acs Photonics*, vol. 4, no. 4, pp. 1009–1014, 2017.

[32] T. Sato, S. H. Matsumoto, M. Konno, Y. Taniguchi, and E. S. Mamishin, "Hitachi's high-end analytical electron microscope: Hf-3300," *Hitachi Review*, vol. 57, no. 3, p. 133, 2008.

[33] J. C. H. S. E. Peter W. Hawkes, *Handbook of Microscopy*. Springer, 2008, ISBN: 978-0-387-34758-5.

[34] C. B. C. David B. Williams, *Transmission Electron Microscopy*. Springer, 2009, ISBN: 978-0-387-76501-3.

[35] M. Bergen *et al.*, "Centralized instrument control for a tem laboratory," *Microscopy and Microanalysis*, vol. 19, no. S2, pp. 1394–1395, 2013.

[36] L. Ju *et al.*, "Graphene plasmonics for tunable terahertz metamaterials," *Nature nanotechnology*, vol. 6, no. 10, pp. 630–634, 2011.

[37] P. Shekhar and Z. Jacob, "Strong coupling in hyperbolic metamaterials," *Physical Review B*, vol. 90, no. 4, p. 045 313, 2014.

[38] D.-D. Wang *et al.*, "A sensitive red light nano-photodetector propelled by plasmonic copper nanoparticles," *Journal of Materials Chemistry C*, vol. 5, no. 6, pp. 1328–1335, 2017.

[39] J. Sanz *et al.*, "Uv plasmonic behavior of various metal nanoparticles in the near-and far-field regimes: Geometry and substrate effects," *The Journal of Physical Chemistry C*, vol. 117, no. 38, pp. 19 606–19 615, 2013.

[40] D. P. Sanders, "Advances in patterning materials for 193 nm immersion lithography," *Chemical reviews*, vol. 110, no. 1, pp. 321–360, 2010.

[41] I Fomenkov, A Schafgans, and D Brandt, "Laser-produced plasma sources for high-volume-manufacturing euv lithography," *Synchrotron Radiation News*, vol. 32, no. 4, pp. 3–8, 2019.

[42] A. Cross *et al.*, "High sensitivity repeater detection with broadband plasma optical wafer inspection for mask defect qualification," in *Extreme Ultraviolet Lithography 2020*, International Society for Optics and Photonics, vol. 11517, 2020, 115170U.

[43] Y. Imamiya, S. AKAMA, Y. FUJITA, and H. NIITANI, "Development of microfabrication technology using duv laser," *Mitsubishi Heavy Industries Technical Review*, vol. 53, no. 4, p. 49, 2016.

[44] Y. Kumamoto, K. Fujita, N. I. Smith, and S. Kawata, "Deep-uv biological imaging by lanthanide ion molecular protection," *Biomedical optics express*, vol. 7, no. 1, pp. 158–170, 2016.

[45] Z. Feng-Feng *et al.*, "A picosecond widely tunable deep-ultraviolet laser for angle-resolved photoemission spectroscopy," *Chinese Physics B*, vol. 22, no. 6, p. 064 212, 2013.

[46] J. A. Scholl, A. L. Koh, and J. A. Dionne, "Quantum plasmon resonances of individual metallic nanoparticles," *Nature*, vol. 483, no. 7390, pp. 421–427, 2012.

[47] H. Philipp and H. Ehrenreich, "Optical properties of semiconductors," *Physical Review*, vol. 129, no. 4, p. 1550, 1963.

[48] J. Heyd, G. E. Scuseria, and M. Ernzerhof, "Hybrid functionals based on a screened coulomb potential," *The Journal of chemical physics*, vol. 118, no. 18, pp. 8207–8215, 2003.

[49] G. Kresse and J. Furthmüller, "Efficient iterative schemes for ab initio total-energy calculations using a plane-wave basis set," *Physical review B*, vol. 54, no. 16, p. 11 169, 1996.

[50] C. Chen, J Silcox, and R Vincent, "Electron-energy losses in silicon: Bulk and surface plasmons and čerenkov radiation," *Physical Review B*, vol. 12, no. 1, p. 64, 1975.

[51] Q. Meng, L. Wu, H. L. Xin, and Y. Zhu, "Retrieving the energy-loss function from valence electron energy-loss spectrum: Separation of bulk-, surface-losses and cherenkov radiation," *Ultramicroscopy*, vol. 194, pp. 175–181, 2018.

[52] V. Ginis, J. Danckaert, I. Veretennicoff, and P. Tassin, "Controlling cherenkov radiation with transformation-optical metamaterials," *Physical review letters*, vol. 113, no. 16, p. 167 402, 2014.

[53] J.-K. So *et al.*, "Cerenkov radiation in metallic metamaterials," *Applied Physics Letters*, vol. 97, no. 15, p. 151 107, 2010.

[54] I. Kaminer *et al.*, "Efficient plasmonic emission by the quantum čerenkov effect from hot carriers in graphene," *Nature communications*, vol. 7, no. 1, pp. 1–9, 2016.

[55] Y. Zhang *et al.*, "Tunable cherenkov radiation of phonon polaritons in silver nanowire/hexagonal boron nitride heterostructures," *Nano letters*, vol. 20, no. 4, pp. 2770–2777, 2020.

[56] S. J. Smith and E. Purcell, "Visible light from localized surface charges moving across a grating," *Physical Review*, vol. 92, no. 4, p. 1069, 1953.

[57] P. Van den Berg, "Smith–purcell radiation from a point charge moving parallel to a reflection grating," *JOSA*, vol. 63, no. 12, pp. 1588–1597, 1973.

[58] P Zhang, Y Zhang, and M Tang, "Enhanced thz smith-purcell radiation based on the grating grooves with holes array," *Optics express*, vol. 25, no. 10, pp. 10 901–10 910, 2017.

[59] A. Gover and Z. Livni, "Operation regimes of cerenkov-smith-purcell free electron lasers and tw amplifiers," *Optics Communications*, vol. 26, no. 3, pp. 375–380, 1978.

[60] CST Studio Suite, *Cst particle studio*, 2021. [Online]. Available: https://www.3ds.com/products-services/simulia/products/cst-studio-suite/?utm_source=cst.com&utm_medium=301&utm_campaign=cst.

[61] L. V. Rodríguez-de Marcos, J. I. Larruquert, J. A. Méndez, and J. A. Aznárez, "Self-consistent optical constants of sio 2 and ta 2 o 5 films," *Optical Materials Express*, vol. 6, no. 11, pp. 3622–3637, 2016.

[62] H. Andrews, C. Boulware, C. Brau, and J. Jarvis, "Superradiant emission of smith-purcell radiation," *Physical Review Special Topics-Accelerators and Beams*, vol. 8, no. 11, p. 110 702, 2005.

[63] M. Bergen *et al.*, "Centralized instrument control for a tem laboratory," *Microscopy and Microanalysis*, vol. 19, no. S2, pp. 1394–1395, 2013.

[64] A. V. Krukau, O. A. Vydrov, A. F. Izmaylov, and G. E. Scuseria, "Influence of the exchange screening parameter on the performance of screened hybrid functionals," *The Journal of chemical physics*, vol. 125, no. 22, p. 224 106, 2006.

[65] H. J. Monkhorst and J. D. Pack, "Special points for brillouin-zone integrations," *Physical review B*, vol. 13, no. 12, p. 5188, 1976.

Appendix A: Transmission Electron Microscope

A.1 Experimental Methods

q-EELS measurements were performed using a Hitachi HF-3300 TEM/STEM with a cold field emission gun (CFEG), a Gatan Image Filter (GIF) Tridiem^{TM} (model 863) and the MAESTRO central computer control system [63]. An electron beam of energy 300 keV is injected normally onto a thin specimen. EEL spectrometer is used to resolve the electron energy loss over a range of 0-18 eV. The energy-momentum loss of the electrons were mapped to the calibrated CCD to obtain the energy-momentum photonic dispersion in the specified range. Our q-EELS captures the surface plasmon dispersion that are not possible with the earlier EELS techniques.

First-principles density functional theory calculations are carried out using Vienna Ab initio Simulation Package [49]. Germanium band structure is calculated through a hybrid functional method with HSE06 functional [64]. To obtain the dielectric function values with a reasonable accuracy, we first perform a single shot GW_0 calculation. A cutoff energy of 180 eV was considered for the expansion of the plane wave basis, and a Γ-shifted $6 \times 6 \times 6$ Monkhorst–Pack [65] grid was used for the sampling of the Brillouin zone with a default Gaussian smearing.

Germanium grating structure as a DUV radiating source is demonstrated based on the simulations using CST Studio by PIC method [60]. Open boundary conditions

are applied on all boundaries of the simulation cell. Electron source is placed on one end of the grating structure which generates electrons with a kinetic energy 20 KeV and an effective current 1.6 mA. The x component of the radiated transient electric field (E_x) is analyzed by Fourier transform to obtain the corresponding spectrum. E_x Spectrum is normalized with respect to the peak amplitude at 8.6 eV.